C. R. Chimie 17 (2014) 775–784

Contents lists available at SciVerse ScienceDirect

Comptes Rendus Chimie

www.sciencedirect.com

Full paper/Mémoire

CO oxidation catalyzed by Ag/SBA-15 catalysts: Influence of the hydrothermal treatment☆

Hadjira Guerba [a,b], Brahim Djellouli [b], Corinne Petit [a], Véronique Pitchon [a,*]

[a] Laboratoire des matériaux, surfaces et procédés pour la catalyse (LMSPC), UMR 7515 du CNRS, université de Strasbourg (UDS), 25, rue Becquerel, 67087 Strasbourg cedex, France
[b] Laboratoire de génie des procédés chimiques (LGPC), université Ferhat-Abbas, 1900 Sétif, Algeria

ARTICLE INFO

Article history:
Received 3 June 2013
Accepted after revision 2 September 2013
Available online 12 December 2013

Keywords:
SBA-15
Silver catalysis
CO oxidation
Silver nano-particles
Double-solvent technique

ABSTRACT

Four types of SBA-15 were prepared with different times and temperatures of treatment in order to obtain a range of micropore sizes. CO oxidation was used as a probe reaction in order to evaluate the nature of the active species when SBA-15s were doped with ca 10% Ag deposited from an $AgNO_3$ solution and calcined or reduced at 350 °C. The texture (TEM, nitrogen physisorption), structure (XRD) and reducibility (TPR) of the various catalysts (Ag/SBA-15) were studied and compared to those of a catalyst prepared by deposition of silver on fumed silica as a reference. These catalysts differ initially by the nature of silica and by pore sizes. In CO oxidation, pre-reduced catalysts are more active than pre-oxidised ones. This has to do with two phenomena, i.e. sintering, which produces large inactive silver particles, and formation of active silver species in the form of small Ag_2O particles.

1. Introduction

Activation of silver catalysts is often regarded as a result of the presence of various Ag–O interactions, for example with molecular oxygen or with surface and subsurface oxygen atoms [1–3]. The performance of silver catalysts depends strongly upon the surface structure and the nature of the active sites, which are very sensitive to the preparation method, the pre-treatment, the reaction conditions and the size of silver nano-particles. The surface and sub-surface oxygen atoms were reported to be the active sites for Ag catalysts in many oxidation reactions [4–7]. The different pre-treatment atmospheres and temperatures affect the formation of sub-surface oxygen and activate silver species. The roles of the different silver species have also been studied and, for the selective catalytic oxidation of ammonia to nitrogen on Ag/Al_2O_3, Ag° was found to be active species which enhance the catalytic activity at low temperature (< 140 °C), in contrast with Ag^{+}, which could be the active species above 140 °C [8].

It is generally accepted that O_2 on oxides undergoes a series of surface reaction steps, during which the solid acts as an electron donor [9,10]:

$$O_{2\,(ads)} \rightarrow O_2{}^{-}{}_{(ads)} \rightarrow O^{-}{}_{(ads)} \rightarrow O^{2-}{}_{(ads)}$$

The surface oxygen species can be characterised by thermodesorption (O_2 – TPD). A typical O_2 – TPD profile may comprise 5 to 6 peaks, ascribed to different surface, subsurface oxygen or even oxide species [11,12].

The catalytic oxidation of CO to CO_2 at low temperature is an important subject for the environmental protection [12], and has widespread applications in air purification for the buildings or cars. In the present work, four silica of SBA-15 type were prepared to serve as supports for 10% silver. They were made up using P123 copolymer as a structure agent in acidic condition with different times and

☆ Thematic issue devoted to François Garin.
* Corresponding author.
E-mail address: pitchon@chimie.u-strasbg.fr (V. Pitchon).

1631-0748/$ – see front matter
http://dx.doi.org/10.1016/j.crci.2013.09.001

temperatures of treatment in order to show the effect of hydrothermal treatment on the distribution and pore size diameter and to evidence the possible effects on the electronic properties of silver using various physical techniques (BET, XRD, TPR) and CO oxidation reaction, which serves as a probe reaction.

Several works in the literature [13,14] provided evidence that micro-porosity could be formed only in samples prepared with an ageing temperature comprised between 35 and 90 °C. No micro-porosity was observed for solids prepared with an ageing temperature above 100 °C. This idea was applied in our work to select the duration of synthesis and the ageing conditions in order to find the best support that can provide stronger confinement. The catalysts were characterised extensively in order to reveal the relationship between CO/O_2 reactivity and the nature of the silver active species, i.e. size and/or oxidation state effects.

2. Experimental

2.1. Synthesis of SBA-15 materials

The meso-structured silica SBA-15 materials were prepared using the hydrothermal procedure as reported by Zhao et al. [15,16]. A typical synthesis of SBA-15 was carried out using the following conditions. Homogeneous dilution of 16.0 g of triblock copolymer Pluronics® P123 (Aldrich) was carried out in 500 ml of an aqueous acidic solution (HCl, 1,9M Sigm – Aldrich) under constant and vigorous stirring at 35 °C during 1 h. Then, 36.6 ml of tetraethylorthosilicate (TEOS, 98%, GPR Rectapur) were added dropwise for 45 min and under the same conditions of temperature and stirring. Gel formation and ageing were carried out at 35 ± 1.5 °C for 24 h. The precipitated white gel obtained was collected and separated in four fraction samples. The first fraction was only filtered and dried, without any hydrothermal treatment. The second was transferred to a polystyrene bottle and then heated under static conditions at 100 °C for 24 h. Similarly, the third fraction was kept under the same hydrothermal conditions and the same temperature for 72 h. The last and fourth fraction was kept in the same static conditions, but at 130 °C for 24 h. Finally, all samples were filtered and dried at room temperature and calcined in air with a flow rate of 200 $cm^3.min^{-1}$ and a heating ramp rate of 2 $°C.min^{-1}$ at 500 °C for 6 h in order to remove the organic template. Some black oil, a residue of the organic template, was trapped at the exit of the vertically disposed calcination reactor.

The four meso-structured materials synthesised were denoted as SBA-15C1 (0 h, 35 °C), SBA-15C2 (24 h, 100 °C), SBA-15C3 (72 h, 100 °C), SBA-15C4 (24 h, 130 °C), corresponding to the duration and the temperature of hydrothermal treatment, respectively. The series of samples are noted SBA-15C.

2.2. Preparation of the catalysts

The supported Ag/SBA-15 C catalysts were prepared according to the "two-solvent" technique reported elsewhere [17,18], in which one gram of the freshly calcined silica is suspended in 70 ml of dry hexane (Sigma – Aldrich) used as a hydrophobic solvent. Then, the desired amount of silver nitrate was dissolved in distilled water and the quantity corresponding exactly to the pore volume of SBA-15C determined by N_2 sorption was added. The solution of metal precursors was added dropwise with a micropipette in less than 3 min. The gel mixture was aged at room temperature for 24 h under vigorous stirring to help the penetration of metallic precursors inside the pores, and all traces of solvents were eliminated. Then the powder was recovered, and finally calcined at 350 °C for 6 h with a heating rate of 2 $°C.min^{-1}$ to obtain the metal oxides. The targeted value of silver loading was 10%. An equivalent loading of Ag was also impregnated on fumed silica (Sigma-Aldrich, $S = 380\ m^2.g^{-1}$) to serve as a reference. This last sample is labelled as Ag/SiO_2.

2.3. Characterisation techniques

N_2 adsorption and desorption isotherms were obtained at 77K using an ASAP Micrometrics system. Before measurement, all samples were outgassed at 250 °C overnight to desorb moisture from the surface. The pore-size distributions were derived from the adsorption and desorption branches of the BET isotherms by applying the BJH method [19]. The specific surface area values were calculated using the BET procedure.

X-ray diffraction (XRD) patterns were recorded on a Bruker D8 Advance diffractometer using monochromatized Cu Kα radiation (λ = 1.5406 Å). The XRD patterns were recorded between 2° and 90° (2θ) using two types of length steps: 0.016° for 0.50 s and 0.02° for 1 s. The phase identifications were made with the help of the files of the Joint Committee on Powder Diffraction Standards (PDF-IC2D).

Scanning Electron Microscopy (SEM) measurements were performed on a JEOL-JSM 6700 F apparatus. TEM micrograph measurements were performed on a Topcom Model EM-002B apparatus; all the samples were dispersed in an ethanol solution and then deposited on a holey carbon film supported on a copper grid.

The silver content in the calcined catalysts and all the chemical elementary analysis were determined at CNRS – Vernaison, Solaize (France).

The reduction of the supported oxidised silver phases was studied by hydrogen temperature programmed reduction (H_2 – TPR) in a Micrometrics Autochem II. About 50 mg of the calcined sample catalyst were flushed with 30 $cm^3.mn^{-1}$ of argon at room temperature for 30 min, after which a mixture of 10 vol. % H_2 in argon was passed through the catalyst bed at a flow rate of 50 $cm^3.min^{-1}$, while the temperature was increased up to 1000 °C with a heating ramp rate of 10 $°C.min^{-1}$. H_2 consumption was monitored by a thermal conductivity detector (TCD), previously calibrated using CuO reduction as a reference.

2.4. Catalytic tests

The catalytic activity and stability of all catalysts were evaluated on a fixed bed microreactor operating under

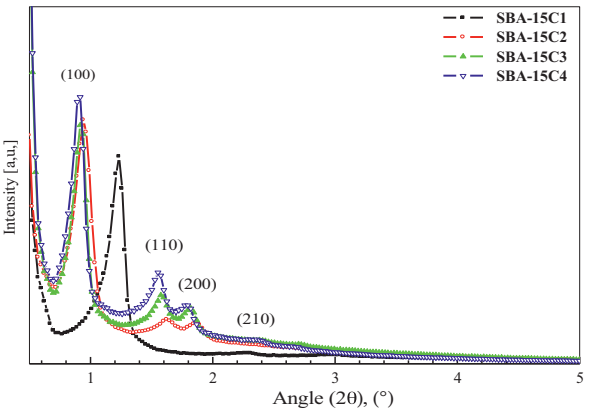

Fig. 1. (Colour online) Small-angle XRD patterns of the four synthesised SBA-15C samples.

Table 1
XRD characterisation of the SBA-15C samples.

Samples	SBA-15C1	SBA-15C2	SBA-15C3	SBA-15C4
2θ	1.22	0.93	0.89	0.91
d_{100} (nm)	7.18	9.41/8.43[a]	9.92	9.64
a_0 (nm)	8.29/11.11[b]	10.87/18.18[b]	11.45	11.13
$a_0 = 2/\sqrt{3} \times d_{100}$				
FWHM	0.13	0.14	0.10	0.11

d_{100}: (100) inter-planar spacing for all calcined samples.
[a] Calculated from the diffraction pattern image of Fourier transform (inset in Fig. 3E).
[b] Approximate value based on the assumption of 2-D hexagonal symmetry that was indicated by TEM (Fig. 3C, E).

atmospheric pressure, packed with 50 mg of catalyst diluted in cordierite. The catalytic oxidation of CO was performed under 1.5% CO and 5% O_2 in helium. The total flow rate was maintained constant at 50 $cm^3.min^{-1}$. The residual amount of CO and CO_2 formed was quantified by an Infrared Rosemount detector. The catalytic tests were performed from room temperature to 500 °C. The experiment was repeated several times in order to determine the reproducibility.

3. Results and discussion

3.1. Supports characterisations

The effect of hydrothermal treatment on the surface area and pore structure parameters of SBA-15 samples is shown by X-ray diffraction patterns (Fig. 1), N2 adsorption–desorption isotherms (Fig. 2), and TEM images (Fig. 3). The low-angle XRD is the only technique that can accurately determine the spacing and goes back to the lattice parameter a_0.

In Fig. 1A are shown the small-angle X-ray diffraction profiles of all the SBA-15 samples. A very intense diffraction peak associated with three additional peaks of lower intensity was resolved, corresponding to the (100), (110), (200) and (210) planes, which are in good agreement with the reported 2D hexagonal ordered structure of SBA-15C type. The presence of three well-resolved peaks and of an additional fourth small one also argues in favour of well-ordered mesoporous materials with a 2D hexagonal pore framework.

The diffraction pattern at small angles indicates the formation of a phase with a 2D hexagonal arrangement with a *p6mm* planar space group and of uniformly sized cylindrical mesopores, and thick-wall analogues to the SBA-15 type.

The position of the diffraction lines of the plan (100) for the support SBA-15C1, without hydrothermal treatment, is slightly shifted toward wide angle values in comparison with the three other materials, which indicates a smaller interplanar distance (Table 1).

The intensity and full widths at half-height maximum allow characterizing the degree of crystallinity. Very small FWHM values (Table 1) for the intense peaks (100) indicate a perfect hexagonal organization for all SBA-15 C samples. According to this criterion, the efficiency of the preparation can be ordered as: SBA-15C3 > SBA-15C4 > SBA-15C1 > SBA-15C2. This classification implies that the degree of pore ordering in the materials prepared under higher temperature conditions is better.

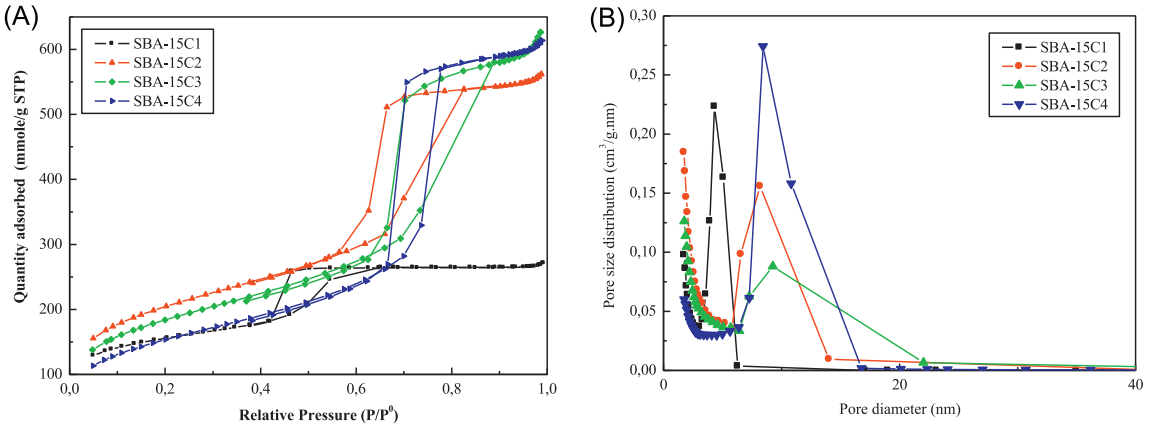

Fig. 2. (Colour online) (A) Nitrogen adsorption–desorption isotherms and (B) pore-size distribution curves for adsorption of SBA-15C samples.

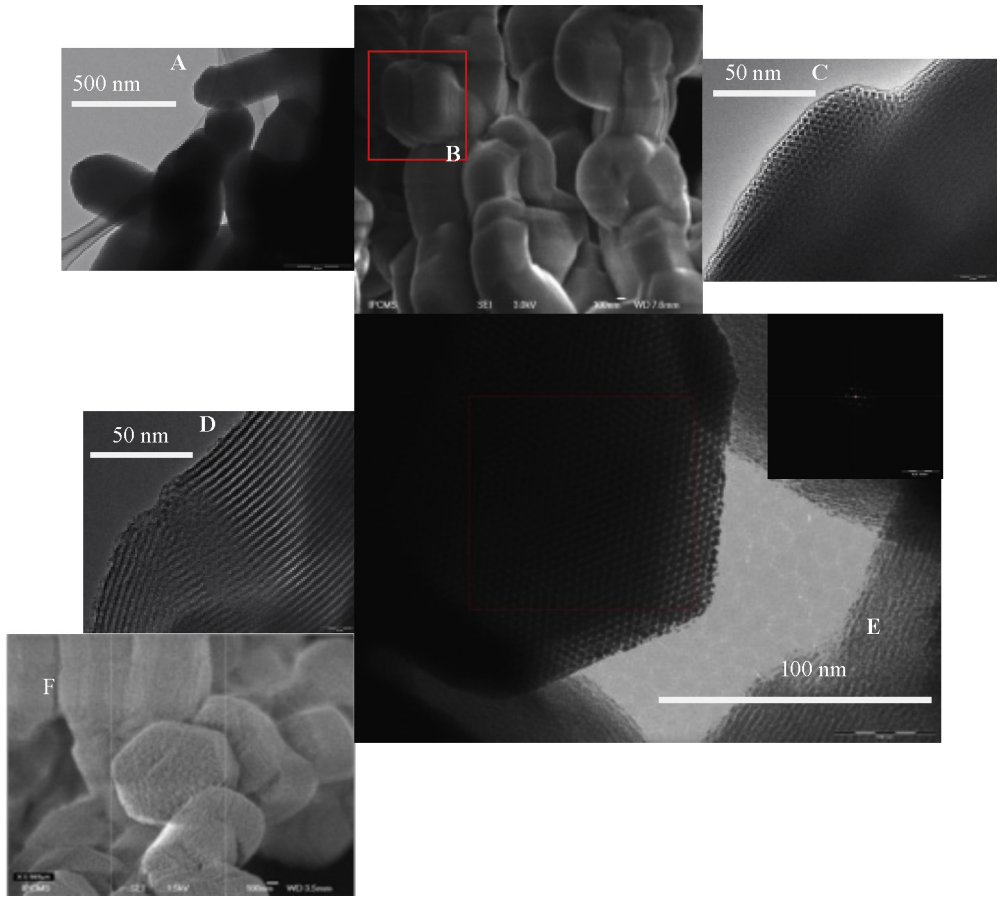

Fig. 3. TEM and SEM images of the SBA-15C samples SBA-15C1 (A–C), SBA-15C2 (D, E) and SBA-15C4 (F).

The walls of silica SBA-15 type consist of amorphous silica; there is a broad single peak at ca. 23°, and no diffraction at large angles (not shown).

N_2 adsorption–desorption isotherms forms and pore size distributions for SBA-15 C supports are shown in Fig. 2 The isotherms observed for all samples are of type IV with an H1-desorption hysteresis loop as defined by IUPAC nomenclature [20], characteristic of mesoporous solids. All SBA-15 C samples have a narrow pore size distribution. SBA-15C1 prepared without hydrothermal treatment has an average diameter of mesopores smaller (4.31 nm) than other samples prepared with a hydrothermal treatment.

The specific area, the pore volume and the mean pore diameter are listed in Table 2.

Table 2
Textural properties of SBA-15C supports.

Samples	SBA-15C1	SBA-15C2	SBA-15C3	SBA-15C4
S_{BET} (m^2/g)	527	718	651	547
V_{PT} (cm^3/g)	0.41	0.86	0.96	0.94
$D_{BJH\ adsorption}$ (nm)	4.31	8.17	9.25	8.42
$D_{BJH\ desorption}$ (nm)	3.61	5.91	6.64	6.68
e_{ads} (nm)	3.98	2.70	2.20	2.71
$e_{ads} = a_0 - D_{BJH\ ads}$				

S_{BET}: BET specific surface area; V_{PT}: total pore volume; D_{BJH}: BJH pore diameter; e_{ads}: pore wall thickness.

For the sample SBA-15C2, the BET area (718 m^2/g) and the pore volume (0.86 cm^3/g) are very similar to the values obtained by several authors [15,21,17]. The Gaussian curve of the pore distribution obtained by the BJH method from the adsorption branch of the isotherm (Fig. 2B) is very narrow and centred at 8.17 nm, 9.25 nm and 8.42 nm for SBA-15C2, SBA-15C3 and SBA-15C4, respectively.

The main pore diameter and the specific surface area increase with the temperature of synthesis (Table 3). The shape of isotherms is in agreement with the mesoporous structure characteristics. An important homogeneity of pore sizes is observed for all samples and the branches of adsorption and desorption curves are parallel, but there are few differences between the hysteresis loops in terms of length and slope, indicating that the SBA-15 C samples prepared with a hydrothermal treatment are characterized by a more homogenous pore size distribution, which supports the XRD results. This might be due to the fact that, for the hydrothermal treatment, such a small temperature of synthesis is insufficient.

It is clear that V_p is very sensitive to the temperature of synthesis. For SBA-15C with HT, the V_p constant is markedly lower, with a value of 0.41 $cm^3.g^{-1}$, while for SBA-15C1 (C2, C3, C4) submitted to a hydrothermal treatment, the values are higher and almost even, ca. 0.96 $cm^3.g^{-1}$. This indicates that the micro-porosity is not

Table 3
Chemical analysis and textural properties of impregnated materials with silver nitrate.

Name	Introduced volume (ml)	Solution concentration (mol/l)	Chemical analysis Ag (%)	S_{BET} (m^2/g)	V_{porous} (cm^3/g)
10% Ag SiO_2	0.432	3	11.29	251	–
10% Ag SBA-15C1	0.432	3	10.30	366	0.26
10% Ag SBA-15C2	0.432	3	10.78	492	0,66
10% Ag SBA-15C3	0.432	3	11.18	540	0.79
10% Ag SBA-15C4	0.432	3	9.77	441	0.75

the only reason explaining the variations of the surface affinity of the SBA-15C samples towards gaseous nitrogen.

The values of pore wall thickness (e_{ads}) significantly decrease when a hydrothermal treatment is applied. Jun et al. have shown the existence of disordered mesopores in the silica walls during the synthesis of carbon molecular sieves using SBA-15 silica as the template [22]. After the removal of the silica template, the pore walls are constructed by disordered carbon networks which replicate the initial structure of the silica. Davidson [23] has confirmed this point by showing that the intensities of the diffraction rays at low angles were very sensitive to the presence of disordered micropores. Therefore, it can be concluded that during the hydrothermal treatment, the formation of a microporous crown around the mesopores occurs, leading to a thinning of the wall thickness, suggesting that the intrawall micropores may form a continuous network that connects adjacent mesopores.

TEM and SEM images (Fig. 3) provide direct observation of the 2D hexagonal ordered mesoporous structure of SBA-15C with a narrow pore size distribution, which is in agreement with the results of XRD and N_2 adsorption–desorption.

3.2. Characterisation of the silver-supported catalysts

The XRD patterns of the silver catalysts are presented in Fig. 4. In all cases, a wide peak is observed at ca. $2\theta = 23^\circ$, attributed to amorphous silica. A comparison with the XRD patterns of parent supports SBA-15 C (Fig. 1) shows only a slight change with three small peaks at about $2\theta = 38$, 44° and 64 that appear in the diffraction pattern of 10% Ag SBA-15C2 and 10% Ag-SBA-15C3 catalysts, corresponding to the diffraction of the cubic lattice of metallic silver (Ag°). A very small line corresponding to Ag_2O appeared at $2\theta = 33^\circ$ for all catalysts.

It should be noted that X-ray diffraction analysis of all samples lasted 15 h, because with a running time of 1 h only, there were no exploitable XRD patterns.

Other species of silver than Ag_2O (small diffraction) are not visible for most of the catalysts; this could mean that the amount of silver deposited onto SBA-15 materials is too low to be observed. However, this should not be the case according to the results of the elemental analysis (Table 3), which prove that there is at least 10% of silver. Therefore, silver should be present in the form of different species either of very small size or constituting an amorphous phase. The first assumption is the most likely, i.e. a high dispersion of silver particles, the absence of diffraction peaks of silver being a good indication of catalytic activity.

The textural properties of different materials SBA-15C modified by silver nitrate using the two-solvents technique are shown in Table 3. N_2 adsorption-desorption isotherms are typical of irreversible type-IV adsorption isotherms with an H1 hysteresis loop, as defined by IUPAC (Fig. 5A).

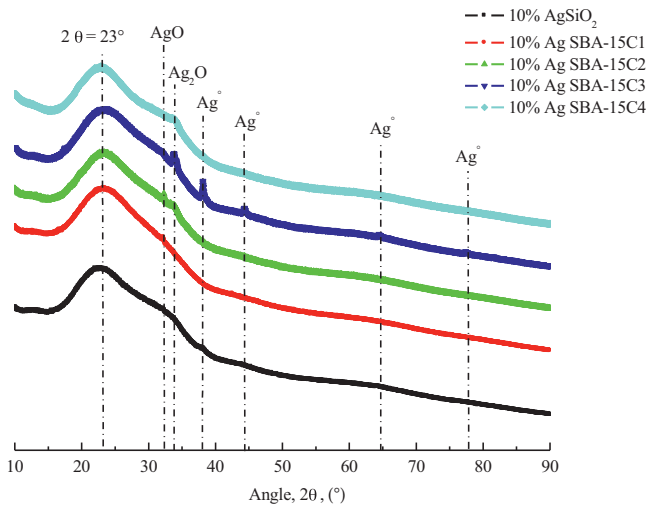

Fig. 4. (Colour online) High-angle XRD patterns of calcined catalysts.

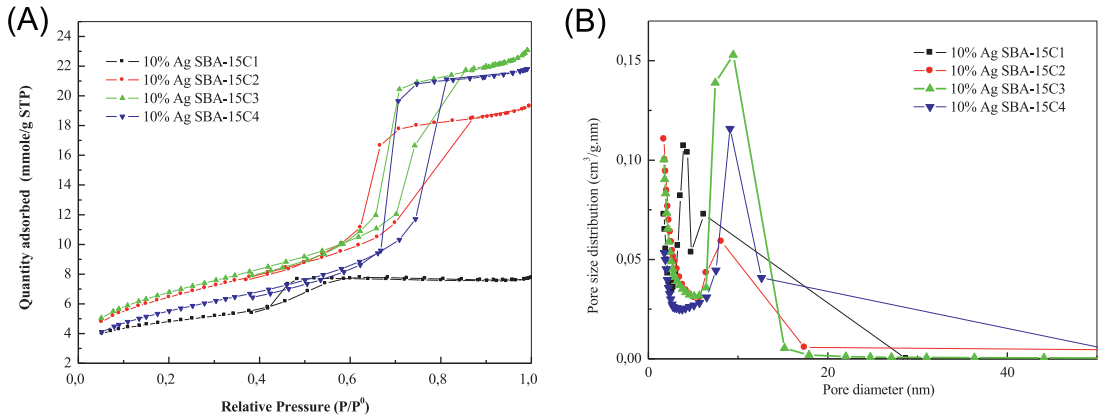

Fig. 5. (Colour online) (A) N_2 adsorption–desorption isotherms of SBA-15C modified by silver. (B) Pore-size distribution curve applied to the adsorption branch.

Impregnation of all SBA-15 materials with silver nitrate produces a decrease in both the specific surface area and the pore volume (Table 3), compared to the initial solids without silver, of c.a. 20 to 25%, which is attributed to the clogging of the pores by silver species, which makes them inaccessible for nitrogen adsorption.

It can be noted, in the case of the 10%Ag SBA-15C1, compared to the parent sample SBA-15C1, the presence of two hysteresis loops that represent an heterogeneous filling by silver. A high-pressure hysteresis is caused by species of silver, probably crystallized, on the external surface, while a low-pressure hysteresis is due to mesopores slightly modified by the insertion of silver species. Two distributions are also observed in the BJH model applied to the adsorption branch (Fig. 5B), a narrow pore-size distribution centred at c.a. 3.9 nm – almost the same size as for the silver-free support – and a novel distribution value centred at 6 nm. The TEM images presented in Fig. 6 confirm this observation (localisation inside and outside the pores).

The TPR profiles for the calcined catalysts are displayed in Fig. 7. They reveal the presence of one or two reduction peaks. According to the sample, the first one is located between 80 and 90 °C, whereas the second one is situated between 110 and 133 °C. Furusawa has observed the same type of reduction at relatively low temperatures in the case of ZSM zeolite doped with silver and has attributed these two peaks to the reduction of large clusters of AgO and

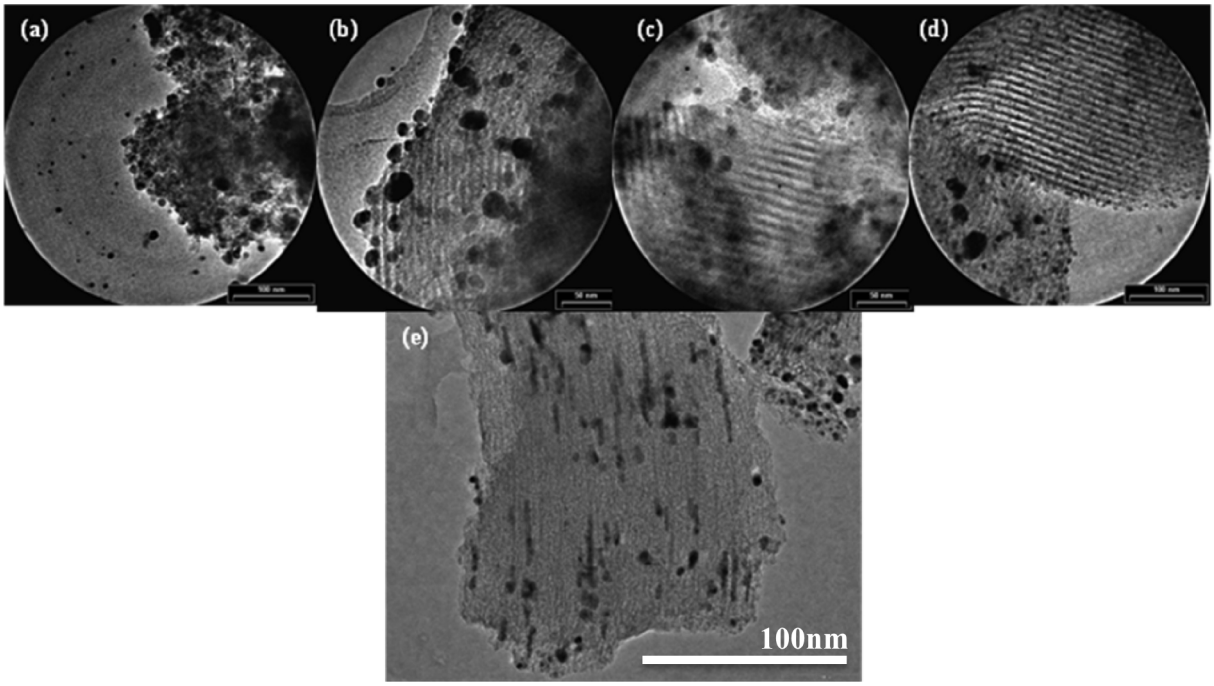

Fig. 6. (Colour online) TEM images of the catalyst (a) $AgSiO_2$, (b) AgSBA-15C1, (c) AgSBA-15C2, (d) AgSBA-15C3 and (e) Ag SBA-15C4.

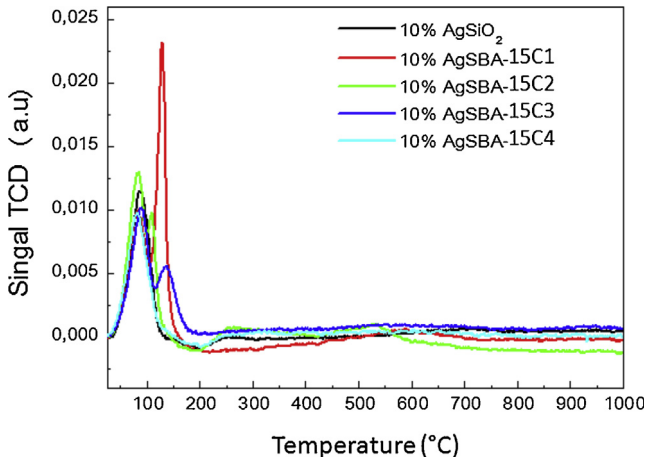

Fig. 7. (Colour online) TPR profiles of calcined catalysts.

Ag_2O located outside the zeolite pores. Conversely, the medium reduction temperature has been assigned to the reduction of small clusters of Ag_2O only [24]. Shimizu has observed the reduction of Ag^+ cations into metallic silver in an Ag–MFI above 400 °C, corresponding to very small clusters of three to four atoms of the type $Ag_{2p}{}^{p+}$ [25]. By analogy with the works in the literature, we have attributed the lowest temperature peak to the reduction of AgO species, AgO being reduced in two steps ($Ag^{+2} \rightarrow Ag^+ \rightarrow Ag^\circ$), whereas the highest temperature peak is characteristic of the reduction of small Ag_2O particles. It is therefore possible to evaluate the percentage of each oxide and, by comparison with the total amount of Ag, the quantity of reduced silver present in the catalysts before TPR can be easily deduced. These values are reported in Table 4. At higher temperatures of TPR, there are no reduction peaks, indicating the absence of species that would be in strong interaction with the support.

The analysis provided by TPR and TEM are in favour of an explanation in which silver species (AgO) were formed on the external surface of silica and created an external porosity, and hence explain the presence of the hysteresis loop at high pressure.

The Ag_2O species are present on SBA-15C obtained at low temperature of treatment: 35 and 100 °C. The amount of Ag_2O decreases with the increase of treatment time and is equal to 11% on Ag/SBA-15C2 and Ag/SBA-15C3. Two catalysts give only a deposition of silver in the micropores (Ag/SiO2) or in the mesopores (Ag/SBA-15C4), as can be seen through the absence of formation of Ag_2O species. If we regard the AgO species as the probe of external deposition, we can consider that silver deposits on the external surface mainly on the Ag/SBA-15C2 and Ag/SBA-15C3 and completely in the case of Ag/SBA-15C4.

All the catalysts contain silver oxides as AgO, Ag_2O and/or metallic silver (Ag°). Table 4 summarizes the total H_2 uptake and the calculated content of AgO, Ag_2O and Ag° for all catalysts. As expected, both catalysts 10% AgSBA-15C4 and 10%$AgSiO_2$ are reduced in a single reduction process at low temperature (at c.a. 88 °C), which corresponds to the reduction of AgO, as proven by the calculated amount of hydrogen (Table 4). The amount of hydrogen consumed is low in comparison with the one obtained on the three others solids, which testify to the fact that the amount of silver oxides is higher in these three catalysts.

Highly ordered-structure SBA-15C with different pore sizes is not affected by the addition of silver nitrate, the structure being preserved, according to the images of catalysts obtained from transmission electronic microscopy presented in Fig. 6. Silver is dispersed as small spherical particles confined inside porosity (image d) or as nanowires (image e). Some dark spots are observed on those images and are attributed to different forms of large-size silver species (AgO), as already detected by TPR, and located outside the pores.

Silver is well dispersed inside the porosity of support SBA-15C4 (image e), SBA-15C3 (image d) and SiO_2 (image a), except for some species of silver (AgO identified by TPR) located at the external surface and/or isolated.

Table 4
Quantification and identification by TPR of the species of silver present in the catalysts.

Catalysts	Ag SiO_2	Ag/SBA-15C1	Ag/SBA-15C2	Ag/SBA-15C3	Ag/SBA-15C4
% Ag	11.29	10.30	10.78	11.18	9.77
H_2 (mmol/g_{cat})	0.26	0.49	0.35	0.32	0.25
% AgO	49.7	22.9	23.7	20.2	55.2
% Ag_2O	0	28.4	11.3	10.7	0
% Ag^0	50.3	48.7	65.0	69.1	44.8

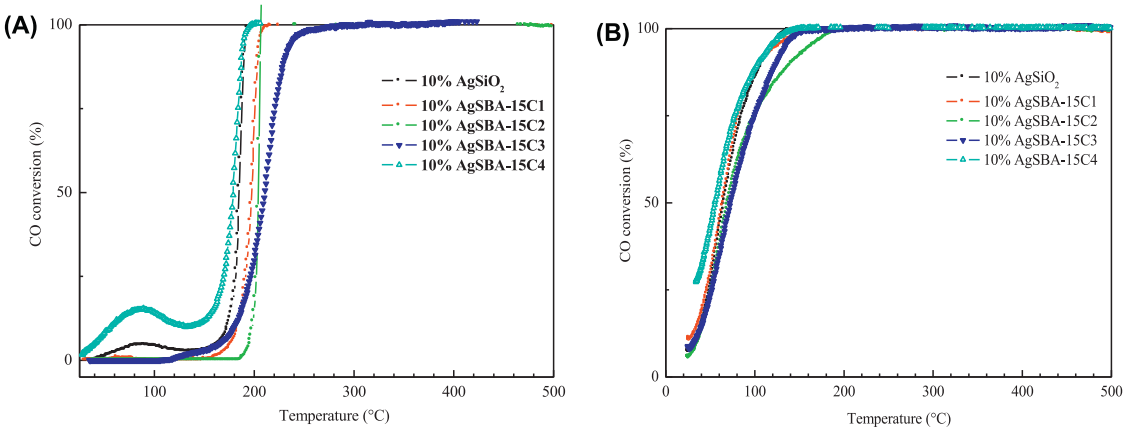

Fig. 8. (Colour online) CO conversion as a function of temperature for silver catalysts supported on SBA-15 and fumed silica SiO_2; (A) silver catalysts calcined at 350 °C (1st run), (B) the same catalysts reduced under hydrogen at 350 °C for 2 h (1st run).

4. Catalytic activity in CO oxidation

4.1. Effect of supports and of pre-treatment

The effect of silver on the supports SBA-15 C with different pore sizes and on fumed silica was evaluated in the total CO oxidation. For the calcined samples, the curves of CO total oxidation are shown in Fig. 8A. As can be seen in this figure, all the catalysts possess very similar activities. The activity is given by the T_{50} value (temperature at which a conversion of 50% is reached) (Table 5).

At room temperature, no activity is observed, although few studies in the literature have shown that silver-based catalysts are able to oxidize CO even below room temperature [26].

Both 10% AgSBA-15C4 and 10% Ag/SiO_2 catalysts lead to a conversion at low temperature (20 and 5% at 85 °C, respectively), but there is a deactivation as the temperature increases. This weak activity of silver-based catalysts at low temperatures ($T < 100$ °C) and the deactivation phenomenon can be related to the presence of species blocking the accessibility of CO to silver crystallites (active sites) confined inside the porosity, according to the evidence provided by TPR and TEM.

Fig. 8B shows the CO conversion as a function of temperature for the reduced catalysts (hydrogen at 350 °C for 2 h and cooling down to room temperature). In this case, conversions of CO are observed even at room temperature, i.e. 8%, 11%, 6%, 8% and 27% for 10%$AgSiO_2$, 10% AgSBA-15C1, 10%AgSBA-15C2, 10% AgSBA-15C3 and 10%AgSBA-154 respectively and the maximum of conversion (100%) is achieved at lower temperature than on oxidised catalysts (less than 300 °C).

4.2. Study of deactivation

In Fig. 9A–E, the conversions of CO to CO_2 either on the calcined or reduced silver are shown. The complete oxidation of CO was carried out in two successive cycles (Table 5). The catalytic activity increases significantly in the second cycle for all calcined catalysts at 350 °C, while it decreases when the catalysts were pre-treated *in situ* with hydrogen; the loss of reactivity depends upon the catalyst (Table 5).

The improved activities observed for the calcined catalysts between two cycles are due to the fact that silver oxide (AgO) is reduced to metallic silver and to the active Ag_2O species in the presence of the reducing atmosphere (CO); all the catalysts exhibit a better catalytic activity. This is proven by the better activity observed for all the catalysts during the second run as compared to the first run (Table 5) and equally by the higher activities observed on the reduced catalysts. A reducing pre-treatment under hydrogen has been systematically carried out to improve the activity.

The rise in the activity for the reduced catalyst as compared to the oxidised catalysts can be explained by an increase in the number of accessible active sites. The most active silver catalyst is SBA-15C4, with a conversion of 27% at room temperature and a total conversion reached at 100 °C. Contrary to the calcined catalysts, a deactivation is observed between the first and the second run for all the catalysts.

The decrease in catalytic activity of the catalysts treated with hydrogen in the second cycle can be explained by the sintering of the silver nanoparticles occurring during the first catalytic test up to 500 °C. Sintering is the loss of

Table 5
T_{50} values for CO oxidation for calcined and reduced catalysts.

Catalysts	Ag SiO_2	AgSBA-15C1	AgSBA-15C2	AgSBA-15C3	AgSBA-15C4
% Ag	11.29	10.30	10.78	11	9.77
T_{50} Calc., 1st run	185	198	205	195	180
T_{50} Calc., 2nd run	82	165	166	175	128
T_{50} Red., 1st run	65	63	63	72	55
T_{50} Red., 2nd run	86	134	89	119	69

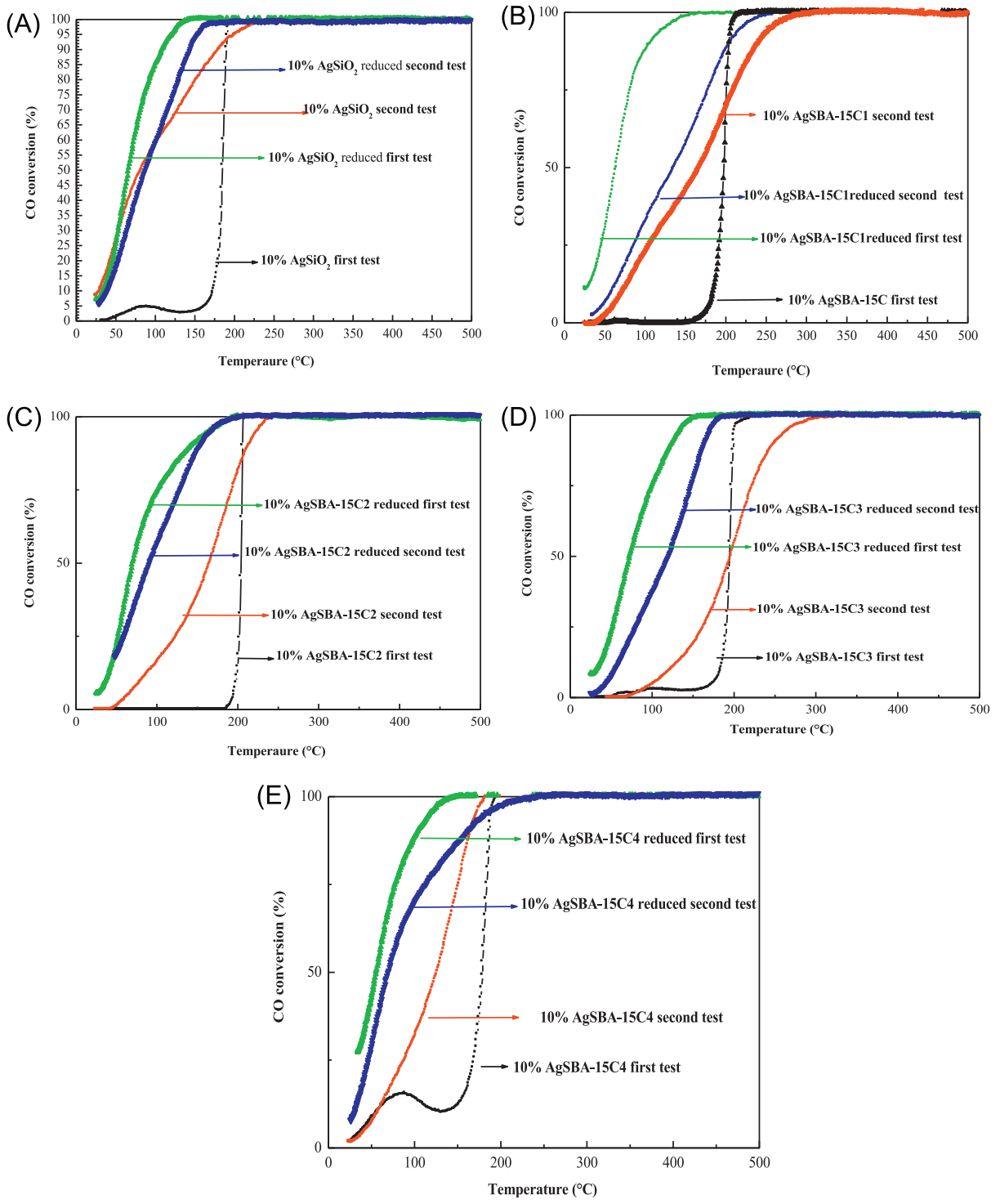

Fig. 9. (Colour online) CO conversion of silver catalysts calcined at 350 °C and then reduced *in situ* under hydrogen (the reaction was carried out in two successive cycles). A, Ag/SiO_2; B, Ag/SBA-15C1; C, Ag/SBA-15C2; D, Ag/SBA-15C3; E, Ag/SBA-15C4.

dispersion of the active phase in which the particles grow by coalescence, this process being directly related to the reaction temperature.

A second explanation would be that silver is active when oxidised, while it becomes much less active when reduced. This explanation should then be put into relation with the activation phenomenon observed at low temperature on the pre-calcined catalysts (10% Ag/SiO_2 and 10% Ag/SBA-15C4). However, this increase in activity of the pre-calcined catalysts is more complex to explain. There is

clearly a state of oxidation in which silver particles are active, an oxidation state that is reached during the first run $CO + O_2$. Several phenomena can explain this activation. It can result from a total elimination of species blocking the access to the active sites during the rise of temperature to 500 °C, for example some traces of Pluronic® that were not burned during calcination. Actually such residual species were identified by IR (not shown); this result has been shown by others authors [27].

In the second test, this activation phenomenon does not occur at low temperatures, but the question raised is to know why this occurs only for two catalysts and not for the others. Therefore, this sole explanation is not sufficient to account for different activation and reaction profiles.

Increased activity is probably the result of a modification of the electronic properties of silver, which goes from a relatively inactive to an active state. However, the reaction gas mixture is strongly oxidizing, i.e. $O_2/CO = 3.3$, which is 6.5 times the value of stoichiometry. Silver is probably oxidized during the course of the reaction. The literature demonstrates that, in general, the reaction is favoured on oxidized silver especially when Ag^+ is in the form Ag_2O, which is considered as being the most active species [28–30].

In every case, the catalysts pre-reduced by hydrogen performed better than the catalysts reduced by CO during the course of the reaction, even when comparing the most active runs, i.e. the first run for reduced catalysts and the second run for oxidised catalysts. This implies that either hydrogen is a better reducing agent than CO and/or that the sintering is more limited with hydrogen than with CO, large silver particles being very stable and therefore inactive for CO oxidation.

5. Conclusion

We have prepared and characterised silver doped SBA-15 with an attempt to control the deposition of silver to make these active and selective materials for CO oxidation. The deposition of silver was carried out by adding a volume solution containing the required amount of metal in regard with the pore volume of SBA-15C silica as measured by nitrogen adsorption–desorption. In terms of quantity and quality, the method is validated because the 10% content of silver was deposited without any loss of metal. Catalysts with contents equal to 10% produce very small silver species as they were not detected by XRD. However, the crystallinity and particles size depend also on the size of the pores. In the case of small pores (SBA-15C1, 3.6 nm), most of the silver is deposited outside the pores, either in the form of silver oxide or metallic silver. In all cases, the destruction of the matrix silica was not observed after silver deposition.

Silver-based catalysts were found active in CO oxidation, which confirms that the deposition of silver was successfully made inside the pores. We found that the pre-reduced catalysts are more active than the pre-oxidized ones. Also, there is an activation of the reaction in the second cycle under the $CO + O_2$ gas mixture in the case of pre-oxidised samples, whereas there is a deactivation in the case of pre-reduced catalysts. These observations allowed us to assume that the active sites consist in silver oxide, probably under the Ag_2O form, in agreement with the literature. This species has also been identified on the surface by TPR. AgO is present in the form of large particles on the external surface, but becomes active upon reduction and reduction into Ag_2O. Large silver particles are inactive for the reaction and remain as spectator species.

References

[1] W.M.H. Sachtler, C. Backex, R.A. van Santen, Catal. Rev. Sci. Eng. 23 (1991) 127–149.
[2] X. Bao, M. Muhler, T. Schedel–Niedrig, R. Schlögl, Phys. Rev. B. 54 (1996) 2249–2262.
[3] X. Bao, M. Muhler, B. Pettinger, R. Schlögl, G. Ertl, Catal. Lett. 22 (1993) 215–225.
[4] X. Bao, M. Muhler, R. Schlögl, G. Ertl, Catal. Lett. 32 (1995) 185–194.
[5] H. Schubert, U. Tegtmeyer, D. Herein, X. Bao, M. Muhler, R. Schlögl, Catal. Lett. 33 (1995) 305–319.
[6] D.S. Su, T. Jacob, T.W. Hansen, D. Wang, R. Schlögl, B. Freitag, S. Kujawa, Angew. Chem. Int. 47 (2008) 5005–5008.
[7] S. Royer, D. Duprez, ChemCatChem 3 (2011) 24–65.
[8] X. Zhang, Z. Qu, X. Li, M. Wen, X. Quan, D. Ma, J. Wu, Sep. Purif. Technol. 72 (2010) 395–400.
[9] M. Che, A.J. Tench, Adv. Catal. 32 (1983) 1–148.
[10] Y. Liu, J. Takei, H. Ohashi, H. He, X. Zhang, M. Haruta, J. Catal. 267 (2009) 121–128.
[11] Y.Z. Wang, Y.X. Zhao, C.G. Gao, D.S. Liu, Catal. Lett. 125 (2008) 134–138.
[12] G.G. Jernigan, G.A. Somorjai, J. Catal. 147 (1994) 567–577.
[13] M. Kruk, M. Jaroniek, C.H. Ko, R. Ryoo, Chem. Mater 12 (2000) 1961–1968.
[14] A. Galarneau, H. Cambon, F.D. Renzo, R. Ryoo, M. Choi, F. Fajula, New J. Chem. 27 (2003) 73–79.
[15] D. Zhao, J. Feng, Q. Huo, N. Melosh, G.H. Frederickson, B.F. Chmelka, G.D. Stucky, Science 279 (1998) 548–552.
[16] P. Yang, D. Zhao, D. Margolese, B.F. Chmelka, G.D. Stucky, Nature 396 (1998) 152–155.
[17] M. Impéror-Clerc, D. Bazin, M.-D. Appay, P. Beaunier, A. Davidson, Chem. Mater. 16 (2004) 1813–1821.
[18] I. Lopes, N.E. Hassan, H. Guerba, G. Wallez, A. Davidson, Chem. Mater. 18 (2006) 5826–5828.
[19] E.P. Barret, L.G. Joyner, P.H. Hallenda, J. Am. Chem. Soc. 73 (1951) 373–379.
[20] K.S.W. Sing, D.H. Everett, R.A. Haul, L. Moscou, R.A. Pierotti, J. Rouquerol, T. Siemieuskra, Pure Appl. Chem. 57 (4) (1985) 603–619.
[21] J. van der Meer, I. Bardez, F. Bart, P.A. Albouy, G. Wallez, A. Davidson, Micropor. Mesopor. Mater. 118 (2009) 183–188.
[22] (a) S. Jun, S.H. Joo, R. Ryoo, J. Am. Chem. Soc. 122 (43) (2000) 10712–10713;
(b) R. Ryoo, C.H. Ko, M. Kruk, M. Jaroniec, J. Phys. Chem. B 104 (2000) 11465–11471;
(c) H.J. Shin, R. Ryoo, M. Kruk, M. Jaroniec, Chem. Commun. (2001) 349–350.
[23] A. Davidson, Curr. Opin. Colloid Interface Sci. 7 (2002) 92–106.
[24] T. Furusawa, K. Seshan, J.A. Lercher, L. Lefferts, K.I. Aika, Appl. Catal. B 37 (2002) 205–216.
[25] J. Shibata, K.I. Shimizu, Y. Takada, A. Shichi, H. Yoshida, S. Satokawa, A. Satsuma, T. Hattori, J. Catal. 227 (2005) 367–374.
[26] W. Gac, A. Derylo-Marczewska, S. Pasieczna-Patkowska, N. Popivnyak, G. Zukocinski, J. Mol. Catal. A 268 (2007) 15–23.
[27] J. Ryczkowski, J. Goworek, W. Gac, S. Pasieczna, T. Borowiecki, Thermochimica Acta 434 (2005) 2–8.
[28] S. Imamura, H.R. Sawada, K. Uemura, S. Ishida, J. Catal. 109 (1988) 198–205.
[29] G.G. Xia, Y.G. Yin, W.S. Willis, J.Y. Wang, S.L. Suib, J. Catal. 185 (1999) 91–105.
[30] Q. Zhenping, C. Mojie, H. Weixin, B. Xinhe, J. Catal. 229 (2005) 446–458.